High Surface Area Montmorillonite−Carbon Composites and Derived Carbons

A. Bakandritsos,[†] Th. Steriotis,[‡] and D. Petridis*[,†]

Institute of Materials Science and Institute of Physical Chemistry, N.C.S.R. Demokritos, Agia Paraskevi 153 10, Athens, Greece

Received October 14, 2003. Revised Manuscript Received February 4, 2004

The intercalation of sugar in smectite clays and the resulting clay−carbon composites after thermal treatment in Ar are described. Sugar activation by H_2SO_4 treatment affords novel clay−carbon composites in which the layer structure of clay is preserved. Combined XRD and TEM measurements strongly suggest that carbonization at 600 °C leads to graphenes distributed over the clay surfaces, forming a nanometric carbonaceous film. Thermal analysis and XRD results show enhanced thermal stability of the clay−carbon composites with the mineral preserving its layered structure even at 900 °C. Acid demineralization of the clay substrate yields novel carbonaceous materials of high surface areas. The templating role of clay substrate in the growth of the carbonaceous layer is revealed by HRTEM micrographs, which show limited packing of graphenes accompanied by improved surface areas. The present clay−carbon composites are low-temperature-synthesized absorbents without the need of high-temperature activation.

Introduction

Smectite clays with a 2:1 mica-like layered structure possess unique intercalation, swelling and ion exchange properties that make possible their restructure to valuable derivatives, like organoclays,[1,2] pillared clays,[3,4] clay nanocrystalline composites,[5,6] and clay−polymer composites.[7−9] Another class of less studied clay derivatives arises from the combination of clays with carbon-based materials, like clay−fullerenes,[10] clay−carbon nanotubes,[11] and clay−active carbon composites. Work on the latter composites, which is the subject of the present paper, is limited. Most of the studies in this area are centered on the use of clay frames as effective templates for shaping novel carbon structures.[12−21] In this respect, monomers, including furfuryl alcohol,[13] acrylonitrile,[18] and vinyl acetate,[20] were first intercalated into clays or pillared clays, followed by interlayer polymerization and finally carbonization at different temperatures under inert conditions. Following removal of the clay template by acid demineralization, interesting graphite-like carbons were isolated and characterized.[20,22,25]

Because the conditions for formation of carbons in clay layers are the same as in the production of active or porous carbons, both carbonaceous materials must be made up of the same basic units. In active carbons the primary units, denoted as graphenes, are flat, polyaromatic molecules generated during the initial step of carbonization of various raw carbonaceous materials in absence of air between 400 and 700 °C. Graphenes contain predominantly carbon and hydrogen, although heteroatoms (oxygen, nitrogen) may be still present in their structure. They are mostly hydrogen-terminated and are arranged in stacks of two to three layers with a more or less parallel orientation forming nano- or

* To whom correspondence should be addressed. Tel: 003 210 6503343. FAX: 003 210 6519430. E-mail dpetrid@ims.demokritos.gr.
[†] Institute of Materials Science.
[‡] Institute of Physical Chemistry.

(1) Theng B. K. G. *The Chemistry of Clay Organic Reactions*; Adam Higker: London, 1974.
(2) Yariv, S.; Cross, H.; Eds. *Organo-Clay Complexes and Interactions*; Marcel Dekker: New York, 2002.
(3) Mitchel, I. V. *Pillared Layered Structures. Current Trends and Application*; Elsevier: London, 1990.
(4) Burch, R. *Catal. Today* **1998**, *2*, 1
(5) Dékány, I.; Turi, L.; Tombácz, E.; Fendler, J. H. *Langmuir* **1995**, *11*, 2285.
(6) Bourlinos, A. B.; Karakassides, M. A.; Simopoulos, A.; Petridis, D. *Chem. Mater.* **2000**, *12*, 2640.
(7) Lagaly, G.; Pinnavaia, T. J.; Eds. *Clay Mineral−Polymer Nanocomposites; Applied Clay Science* **1999**, *15*.
(8) Pinnavaia, T. J.; Beall G. W. *Polymer−Clay Nanocomposites*; J. Wiley & Sons: New York, 2001.
(9) Giannelis, E. P. *Adv. Mater.* **1996**, *8*, 29.
(10) Mehrota, V.; Giannelis, E. P.; Ziolo, R. F.; Rogalskyj, P. *Chem. Mater.* **1992**, *4*, 20.
(11) Gournis, D.; Karakassides, M. A.; Bakas, T.; Boukos, N.; Petridis, D. *Carbon* **2002**, *40*, 2641.
(12) Putyera, K.; Bandosz, T. J.; Jagiello, J.; Schwarz, J. A. *Carbon* **1996**, *34*(12), 1559.
(13) Bandosz. T. J.; Jagiello, J.; Putyera, K.; Schwarz, J. A. *Chem. Mater.* **1996**, *8*, 2023.
(14) Winans, R. E.; Carrado, K. A. *J. Power Sources* **1995**, *54*, 11.
(15) Sandi, G.; Winans, R. E.; Carrado, K. A. *J. Electrochem. Soc.* **1996**, *143*(5), 195.
(16) Sandi, G.; Thiyagarajan, P.; Carrado, K. A.; Winans, R. E. *Chem. Mater.* **1999**, *11*, 235.
(17) Sonobe, N.; Kyotani, T.; Tomita, A. *Carbon* **1991**, *29*(1), 61.
(18) Kyotani, T.; Sonobe, N.; Tomita, A. *Nature* **1988**, *331*, 331.
(19) Sonobe, N.; Kyotani, T.; Tomita, A. *Carbon* **1988**, *26*(4), 573.
(20) Sonobe, N.; Kyotani, T.; Tomita, A. *Carbon* **1990**, *28*, 483.
(21) Sonobe, N.; Kyotani, T.; Hishiyama, Y.; Shiraishi, M.; Tomita, A. *J. Phys. Chem.* **1988**, *92*, 7029.
(22) Meyers, C. J.; Shah, S. D.; Patel, S. C.; Sneeringer, R. M.; Bessel, C. A.; Dollahon, N. R.; Leising, R. A.; Takeuchi, E. S. *J. Phys. Chem. B* **2001**, *105*, 2143.
(23) Xing, W.; Xue, J. S.; Dahn, J. R. *J. Electrochem. Soc.* **1996**, *143*(10), 3046.
(24) Putyera, K.; Bundosz, T. J.; Jagiello, J.; Swartz, J. A. *Clays Clay Minerals* **1994**, *42*, 1.
(25) Zhu, H. Y.; Vansant, E. F.; Ly, G. Q. *J. Colloid Interface Sci.* **1999**, *210*, 352.

10.1021/cm0350030 CCC: $27.50
Published on Web 03/16/2004

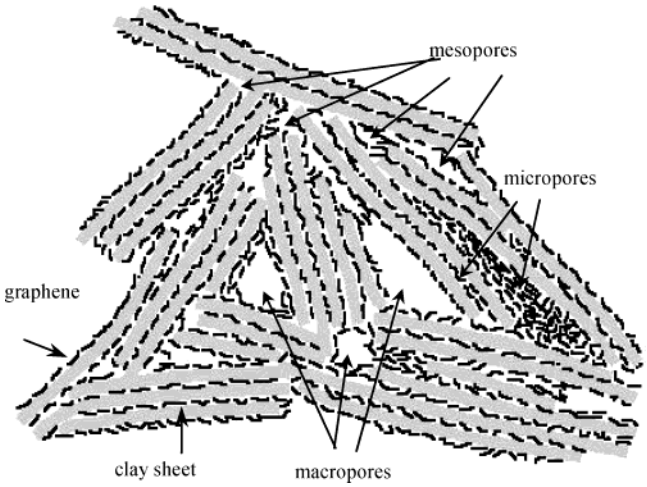

Figure 1. Possible structure of a clay−carbon composite material.

microdomains. However, it is also possible to retain at their edges aliphatic fragments that can stand free or cross-link adjacent sheets. Such arrangements prevent stacking and create regions of disordered or disorganized carbons.[26] Following the "house of cards" concept, originally coined to describe the exfoliated state of phyllomorphic clay minerals through edge to face and edge to edge interactions,[27] it has been proposed that disordered or hard carbons adopt similar microstructures that impart to them better sorptive properties by increasing the accessible surfaces to host molecules.[28,29]

On the other side, smectite clays share with graphenes a common layered structure that could advance their mutual combination to form clay−carbon hybrid nanocomposites. In addition, the unique intercalation and ion exchange properties of smectites provide easy routes for the insertion of various carbogenic precursors between the clay layers. Thermal treatment could transform such clay derivatives into clay−carbon hybrids, in which the clay layers can sustain the assembly of several graphene sheets for the creation of micropores, while other domains derived from house of cards arrangements could provide mesoporosity or even macroporosity, as shown schematically in Figure 1. These hybrid solids hold the promise of important applications, such as catalysts and catalyst supports, gas sorption/separation,[13,25] waste absorbents, liquid decolorizers, and anode materials in lithium batteries.[22] Furthermore, the clay properties offer the possibility to load the clay surfaces with various metal ions or metal oxide catalysts[30] that can add further technological value to the composites.

In an attempt to further investigate the pairing of clays with carbons, the present work describes the synthesis, characterization, and microstructure of clay−carbon composites and also of the carbons derived from them. In a forthcoming publication, the sorbing properties of the clay−carbon composites will be described.

(26) Dahn, J. R.; Zeng, T.; Liy, Y.; Xuw, J. S. *Science* **1995**, *270*, 590.
(27) Van Olphen, H. *An Introduction to Clay Colloid Chemistry*, 2nd ed.; Wiley: New York, 1997; pp 95−98.
(28) Liu, Y.; Xuw, J. S.; Tao Zeng; Dahn J. R. *Carbon* **1996**, *40*(2), 193.
(29) Dahn, J. R.; Buiel, E. R. *Carbon* **1999**, *37*, 1399−1407.
(30) Pinnavaia, T. J. *Science* **1983**, *220*, 365.

Experimental Section

Materials. The montmorillonite used in this study was from the island of Milos, Greece, with the code name Zenith-N and the following chemical composition:

$$Na_{0.63}K_{0.07}Ca_{0.11}\{Si_{7.75}Al_{0.25}\} \times \{Al_{3.21}Mg_{0.69}Fe^{3+}{}_{0.05}Ti_{0.05}\}O_{20}(OH).$$

The sample was fractionated to 2 μm by gravity sedimentation and purified by standard methods.[31] The cation-exchange capacity of Na^+-Montmorillonite, denoted as Z-Na^+, is equal to 80 mequiv/100 g. Common commercial table sugar was used as the carbon source for the fabrication of the composites.

Sample Preparation. Three different clay−sugar derivatives were prepared. The first involved simple intercalation of sugar into Z-Na^+ as follows: 20 mL of a 3% sucrose solution was added to 10 mL of a 5% Z-Na^+ aqueous suspension. After 20 min of stirring, the mixture was dried at 60 °C and finally inserted into a fixed bed flow reactor and pyrolyzed at 600 °C for 1 h under Ar flow. The second sample was prepared by the same procedure, but at the step of sucrose intercalation 600 mg of 97% H_2SO_4 was added to the mixture. After 20 min of stirring, the mixture was dried in air at 60 °C and finally pyrolyzed as before. The third sample was also prepared in the presence of H_2SO_4, but after drying at 60 °C, the solid was washed well with water to remove any excess of the acid before further heat treatment. Each sample, after pyrolysis, was treated with a mixture of HCL and HF (12% and 13%, respectively) for demineralization in order to obtain the pure carbon phase.[13,20] In this step, Teflon vials were used that resist the corrosive action of HF. In Table 1 the identity of samples and their abbreviations are shown. For comparison, carbon from pure sugar, which was treated with H_2SO_4 and pyrolyzed without previous washing of H_2SO_4, was also prepared.

Characterization Methods. Films for X-ray diffraction analysis were prepared by settling a sample suspension on glass plates and drying at room temperature. When films were not formed, powder X-ray diffractograms were obtained. A Siemens D-500 difractometer with Cu Kα radiation was used. N_2 adsorption experiments at −196 °C were performed on an Autosorb-1 gas analyzer with micropore upgrade (Quantachrome Corp.). Samples were outgassed for 5 h at 180 °C under high vacuum. The surface areas were calculated from the Brunauer−Emmett−Teller (BET) and Dubinin−Radushkevich−Kaganer (DRK) equations, and the micropore volume was determined by means of the Dubinin−Radushkevich (DR) approach. The total pore volume was assumed to be the liquid volume of nitrogen at a relative pressure 0.99. Estimates of the micropore and mesopore size distributions were deduced by means of the Dubinin−Astakhov (DA) and Barrett−Joyner−Halenda (BJH) methods, respectively. Thermal analysis experiments were performed using a MOM Q-1500 Derivatograph and 100 mg of each sample in N_2 stream with heating rate of 5 °C/min. Transmition electron microscopy (TEM) and high-resolution TEM measurements were performed on a Philips CM20 electron microscope with an applied acceleration voltage of 200 kV.

Results and Discussion

Intercalation of Sugar into Montmorillonite and Characterization of Intermediates and Composite Products. Table sugar is a disaccharide composed of one glucose and one fructose molecule with the structural formula shown in Figure 2a. Because of its abundance, purity, low cost, and mostly its high carbon yield,[32] it has been proved a convenient source of carbon.[23,29,33,34] Sugar treated with H_2SO_4 undergoes

(31) King, R. D.; Noceda, D. G.; Pinnavaia, T. J. *Electroanal. Chem.* **1987**, *236*, 43.

Table 1. Abbreviation and Identity of the Synthesized Products

composites		derived carbons	
Z-Na^+/C	montmorillonite/carbon composite with no addition of H_2SO_4	carbon	from the composite with no addition of H_2SO_4
Z-H^+(w)/C	montmorillonite/carbon composite in the presence of H_2SO_4 with washing	w-carbon	from the composite with addition of H_2SO_4 and with washing prior to pyrolysis
Z-H^+(uw)/C	montmorillonite/carbon composite in the presence of H_2SO_4 without washing	uw-carbon	from the composite with addition of H_2SO_4 and without washing prior to pyrolysis
sug-H^+/600	sucrose impregnated with H_2SO_4 and carbonized at 600 °C without washing		

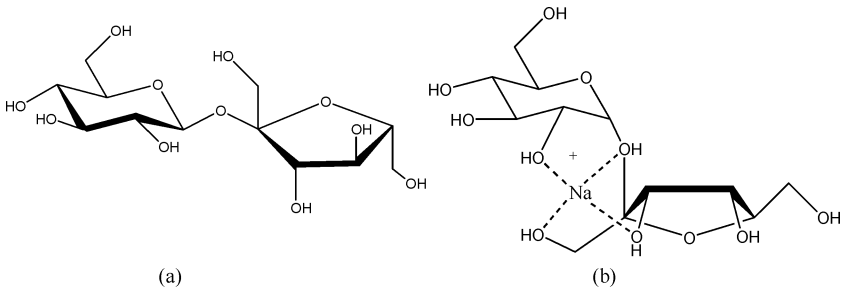

Figure 2. (a) Normal flat orientation of sucrose and (b) complex formation with sodium cations present in the interlamellar space of montmorillonite as counterions (from ref 37).

dehydration and partial polymerization to afford a sugar-char.[35] Pyrolysis of sugar that is pure or activated with H_2SO_4 in an inert atmosphere at temperatures from 600 to 1200 °C yields carbon networks with microporous and mesoporous architectures and high capacity for reversible Li intercalation.[23] In the present work, the fabrication of clay−carbon composites was attained via thermal degradation of clay−sugar derivatives. These derivatives were obtained in two different ways according to the treatment without H_2SO_4 or with H_2SO_4.

Without H_2SO_4. Sugar is readily intercalated into hydrophilic clay surfaces from aqueous dispersions of sodium montmorillonite. Preliminary experiments showed that intercalated sugar is readily displaced from the interlayers by water. An indication of this removal is the decrease in the observed basal spacing values upon water washing. The d_{001} spacing was found to decrease from 19 Å, for an unwashed sample, to 16.9 Å after one washing and to 15.3 Å after three washings. For this reason, the clay−sugar derivatives were dried without water washing after the insertion reaction. The amount of sugar introduced into clay surfaces from sugar solutions of varying concentrations can be estimated from the characteristic XRD reflections of crystalline sugar deposited on the external clay surfaces during drying. To this aim, the aqueous mixtures from clay−sugar intercalates with possible excess of sugar were spread on glass plates and dried at 60 °C for 48 h. The received XRD patterns at different sugar/clay ratios are shown in Figure 3. The results indicate that crystalline sugar reflections are absent near the 1:1 weight ratio. In addition to these results, the d_{001} basal spacing varied with the concentration of sugar used in the intercalation reactions, as shown in Table 2. It is seen that the d_{001} values remained constant around 18.5 Å

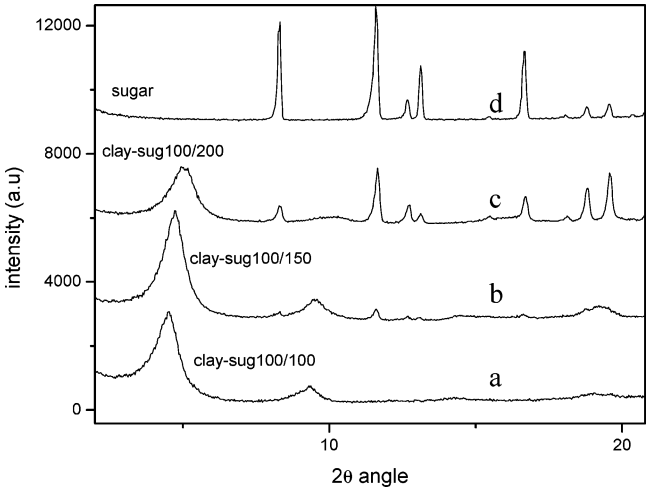

Figure 3. XRD patterns of clay−sugar complexes with different ratios of clay to sugar (a−c) and of pure sugar (d).

Table 2. Dependence of d_{001} of Montmorillonite Layers upon Different Loadings in Sucrose

sugar/clay ratio (w/w)	0.08	0.3	0.6	1.0	1.2	3.0	5.0
d_{001}-spacing (Å)	16.9	18.4	18.5	19.1	19.0	18.9	18.5

for a sugar to mineral weight ratio between 0.3 and 0.6, attained the highest value at 19.1 Å for a 1.0 w/w ratio, and then dropped off at higher sugar concentrations. The XRD results suggest that sugar intercalation should be conducted at a sugar-to-clay ratio of 1. In our preparations we have chosen to use a 20% sugar excess in order to increase the yield of porous carbon in the final clay−carbon composites.

When samples of clay−sugar complexes were heated in air at different temperatures, the color of the resulting solids darkened progressively and the basal spacing decreased (Figure 4), due to the thermal decomposition of the absorbed sugar. At 600 °C (Figure 4e), the carbohydrate was completely burnt out, as evidenced from the light color of the remaining solid and the depression of the silicate thickness to the collapsed value of 9.5 Å. On the contrary, calcination of the clay−sugar complex under Ar at 600 °C gave a black clay−carbon

(32) Pinnavaia, T. J.; Thorpe, M. F.; Eds. *Access in Nanoporous Materials*; Plenum Press: New York, 1995; p 39.
(33) Zhibin, Lei; Yugen, Zhang; Hua, Wang; Yanxiong, Ke; Jianmin, Li; Fanqing, Li; Linyun, Xing, *J. Mater. Chem.* **2001**, *11*, 1975.
(34) Ryong, R.; Sang, H. J.; Shinae, J. *J. Phys. Chem. B* **1999**, *10*(37), 7743.
(35) Yu, J.-S.; Yoon, S. B.; Chai, G. S. *Carbon* **2001**, *39*, 1421.

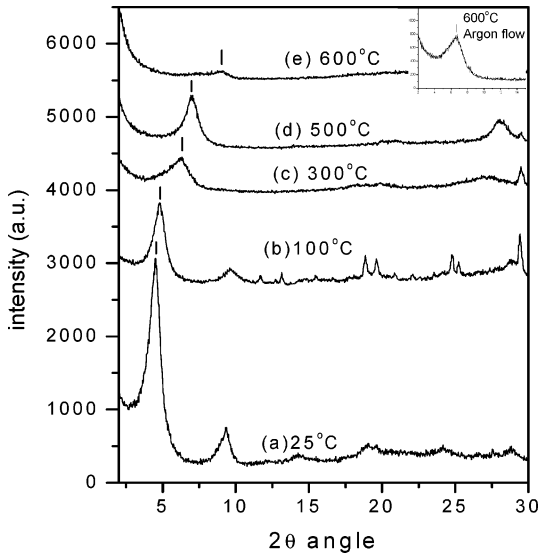

Figure 4. Clay−sugar complexes heated in air at different temperatures with d_{001} progressively diminishing: (a) 19.1 Å, (b) 15.5 Å, (c) 14 Å, (d) 12.1 Å, (e) 9.5 Å. Inset: clay−sugar, 600 °C under Ar, 13.4 Å.

composite, in which the layered structure of the mineral is preserved, as indicated by the presence of the d_{001} spacing at 13.4 Å (inset in Figure 4).

With H_2SO_4. The second preparation route involves the addition of H_2SO_4 to the clay−sugar mixture at the stage of intercalation. The acid activates the clay by transforming it to the high acidity H^+ form and, simultaneously, dehydrates the sugar. During drying of the mixture at 60 °C, the solid turned black, indicating the start of condensation and polymerization of the intercalated and deposited sugar. Subsequently, this black mixture was washed with water or left unwashed. The reason for leaving the product unwashed was the prospect of synthesizing composite materials of higher porosity, as a result of the action of sulfur oxides, liberated during pyrolysis, on the formed carbon layers and on the mineral texture. Besides this action, the acid can transform sugar to a hard carbon precursor by introducing cross-linking bonds in the structure during polymerization. This prevents extensive face-to-face graphene stacking and blocking of free volume and therefore improves the composite's features for sorptive and other applications.[26]

XRD results from the two sets of derivatives (washed and unwashed) pyrolyzed at different temperatures are shown in Figure 5. The clay−sugar/H_2SO_4 precursor dried at room temperature gave a d_{001} basal spacing of 15.8 Å, implying intercalation of sugar to the H^+-form of the mineral, considering that sucrose has an average dimension of 5 Å[36] (Figure 5a). The different d_{001} values for intercalation of sugar in the presence (15.8 Å) and in absence of H_2SO_4 (19.1 Å) (Figure 4a) could be attributed to the different configuration of sucrose in the interlamelar space than to the amount of intercalated sugar. The disaccharide of sucrose is known to form complexes with metal cations,[37] such as Na^+ ions, which in the clay structure are the counterions for the

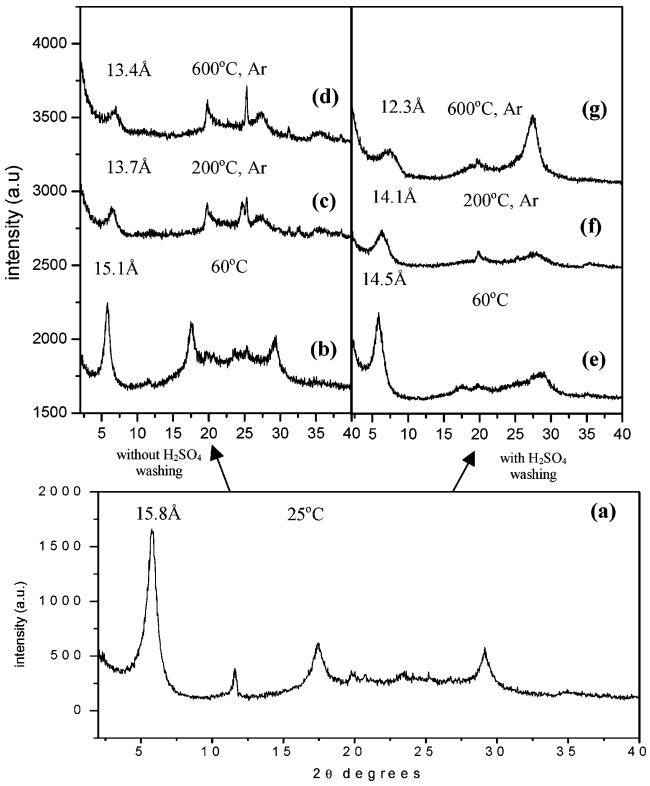

Figure 5. XRD patterns of clay/sucrose/H_2SO_4 products: (bottom) dried at 25 °C, (left part) (b−d) without and right part (e−g) with H_2SO_4 washing; samples were thermally treated at indicated temperatures.

negatively charged layers. Formation of such complexes leads to an expansion of sucrose unit cell dimensions from a = 10.863 Å, b = 8.705 Å, and c = 7.758 Å for sucrose[38]to a = 17.177 Å, b = 8.388 Å, and c = 29.696 Å for a complex with Na^+ ions,[39] explaining the higher d_{001} spacing of Z-Na^+/sugar complex. We note that in both cases the unit cell consists of two molecules of sucrose, so the cell constants should be divided by two in order to be compared with the interlamellar spacings. After this, constant a fits very well to the experimental values, if we also take into account a hydration sphere around sucrose or a sucrose−Na^+ complex. In presence of H_2SO_4, the Na^+ cations are displaced by H^+, causing the destruction of Na^+ complexation and leading to a flat configuration of sucrose (Figure 2a,b).

The unwashed sample, dried at 60 °C, shows a higher d_{001} spacing compared to the washed sample (patterns b and e in Figure 5), which can be explained from leaching of sucrose monomers or oligomers during washing. On the other hand, at 200 °C the situation is reversed (patterns c and f in Figure 5) and the smaller d_{001} value corresponds now to the unwashed intermediate. This is because sulfuric acid accelerates the carbonization process[40] and decomposition of sucrose to graphenes starts at lower temperatures. It is important to note that all XRD patterns show clearly the d_{001} reflection from the clay layers between 5° and 7.5° 2θ,

(36) Monteiro, C.; Herve du Penhoat, C. *J. Phys. Chem. A* **2001**, *105*, 9827

(37) Karlin, K. D. *Progress in inorganic chemistry*; John Willey & Sons: New York, 1977.

(38) Donnay, J. D. H.; Kennard, O.; Watson, D. G.; Rodgers, J. R.; Eds. *Crystal Data-Determinative Tables: organic compounds*; JCPDS-International Centre for Diffraction Data, 1978; Vol. 3.

(39) Accorsi, C. A.; Bertolasi, V.; Ferreti, V.; Gilli, G. *Carbohydr. Res.* **1989** *191*(1), 91.

(40) Kirck, R. E.; Othmer, D. F. *Encyclopedia of Chemical Technology* 2, 3rd ed.; New York, 1960.

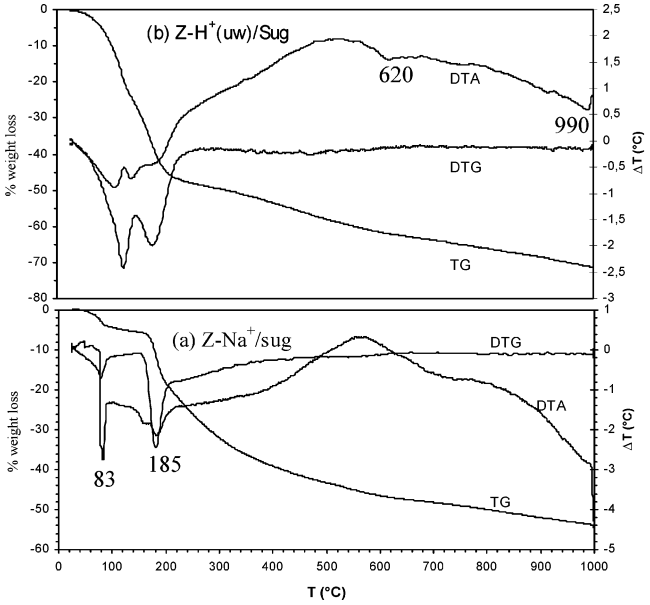

Figure 6. TG, DTG, and DTA curves of (a) Z-Na^+/sugar precursor and (b) montmorillonite/sugar/H_2SO_4 precursor.

implying that the mineral preserves its layered structure during pyrolysis, irrespective of washing H_2SO_4 out or not prior to pyrolysis. This result is also supported by TEM measurements, as will be discussed later. Finally, it is well-known in clay science that H_2SO_4 in appropriate concentrations and conditions causes first the extraction of lattice metal cations from clay layers and finally dissolution of the mineral. The observed values of 12.3 Å (washed) and 13.4 Å (unwashed) for the thermally treated at 600 °C composites reflect the extra stability of the aluminosilicate structure attained by the incorporation of graphene layers between the aluminosilicate structure. Furthermore, considering that the thickness of pyrene, a flat molecule resembling the graphene structure, is 3.5 Å[41] and that the clay layer measures to near 9.5 Å, we conclude that the observed 001 values point to the incorporation of one graphene layer between the clay surfaces.

Thermal Analysis. Turning to the thermal analysis results for the Z-Na^+/sugar and Z-Na^+/sugar/H_2SO_4 derivatives (Figure 6), a first weight loss at 83 °C in TG, reflected also by a corresponding peak in the DTG and an endothermic peak in DTA curves, corresponds to vaporized water loosely bound to montmorillonite.[42] The second weight loss at 185 °C, which is the melting point of sucrose, is attributed to its dehydration and caramelization processes. A DTG peak and an endothermic DTA peak also indicate these changes. Another small endothermic peak, visible only in the DTA curve, might come from an endothermic change in the crystal structure of the commercial table sugar. The weight loss at higher temperatures can be attributed to the vaporization of water, which is strongly absorbed by the clay, and to CO_2, CH_4, and CO emissions from the carbonization process of sucrose.[23] Above 600 °C, the weight loss continues because of further elimination of oxygen and hydrogen from sucrose molecules.

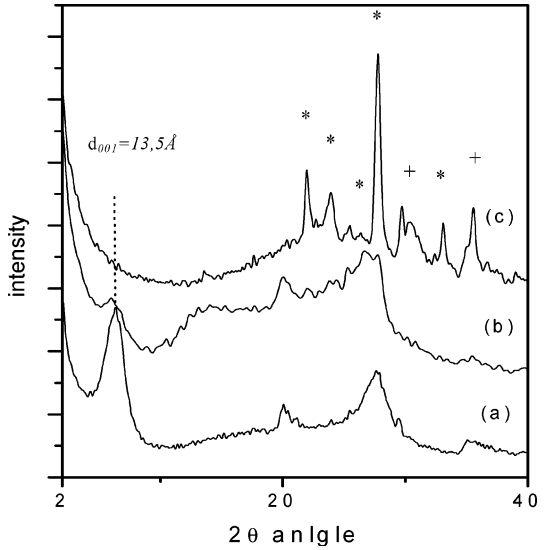

Figure 7. XRD patterns of (a) composite Z-Na^+/C, (b) the same composite after thermal treatment at 900 °C under Ar, and (c) montmorillonite after thermal treatment at 900 °C under argon flow. The dotted line designates the (001) reflection of montmorillonite; the stars correspond to Si, Al, and mixed Si/Al oxides and the crosses to Fe oxides.

When smectites or other clays are thermally treated, two endothermic peaks at 620 and 850 °C appear in the DTA curves, arising from dehydroxylation of the clay structure, and one exothermic peak at about 900 °C appears from degradation and recrystallization of the clay lattice.[42] These peaks are absent from the DTA curve of the Z-Na^+/sugar sample (Figure 6a), whereas for the Z-H^+(uw)/sug sample the two endothermic peaks are present, with the second being shifted from 850 to 990 °C, and the exothermic peak at 900 °C is missing (Figure 6b). Considering that this exothermic peak appears in other clay derivatives with organic matter, for example in a clay/catechol derivative,[42] we attribute its absence to an enhanced stability imparted to the clay structure by the presence of graphenes in its layers. For further verification of this stability, untreated Z-Na^+ and the composite Z-Na^+/C, were subjected to thermal treatment at 900 °C for 1 h in Ar, and the corresponding XRD diagrams were obtained (Figure 7a−c). The composite Z-Na^+/C retained the 001 reflection from the parallel stacking of the clay layers, while Z-Na^+ lost its lamellar structure, as evidenced from the absence of 001 reflection and from the appearance of several other peaks in the region of 20−40° 2θ from Al and Si oxides, mixed Al/Si oxides, and Fe oxides. Increased thermal stability has been previously noted for pillared clay/carbon composites, but in this case the thermal stability may arise from pillaring of the clay structure.[43,44]

From TG measurements of the composites in oxygen atmosphere (provided in Supporting Information), we calculated their carbon content. In the case of Z-Na^+/C it was found to be 32%, while it was 29% for Z-H^+(uw)/C and 26% for Z-H^+w/C. The smaller amount of carbon in the composite Z-H^+(w)/C is expected because of leaching of sucrose during the washing step. Finally, pyrolysis of sucrose in Ar yields 28% carbon.

(41) Wiederrecht, G. P.; Sandi, G.; Carrado, K. A.; Seifert S. *Chem. Mater.* **2001**, *13*, 4233.
(42) Mackenzie, R. C. *The Differential Thermal Investigation of clays*; Mineralogical Society: London, 1957.
(43) Brindley, G. W.; Sempels, R. E. *Clay Minerals* **1997**, *12*, 229.
(44) Pinnavaia, T. J.; Zhou, M. S.; Landau, S. D.; Raythatha, R. H. *J. Mol. Catal.* **1984**, *27*, 195.

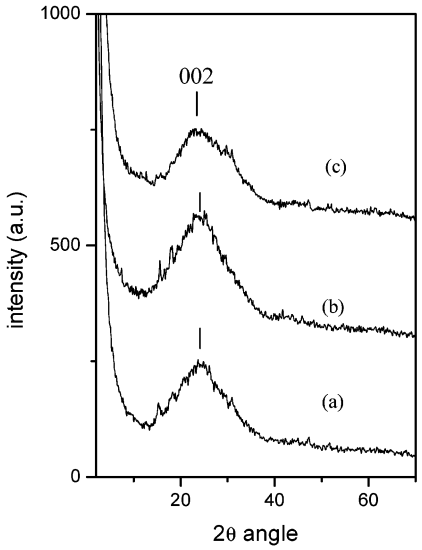

Figure 8. XRD patterns of carbons derived after dissolution of the inorganic matrix: (a) carbon, $d_{002} = 3.65$ Å, (b) w-carbon, $d_{002} = 3.65$ Å, and (c) uw-carbon, $d_{002} = 3.75$ Å

Carbons from the Clay-Carbon Composites and Their Characterization. Treatment of the montmorillonite/carbon composites with a mixture of HCL and HF dissolves the inorganic substrate and affords the carbon phase free of the aluminosilicate mineral and without any significant changes in its structure.[13,20] The derived carbons gave XRD patterns with a broad peak in the 2θ region of 20−30° corresponding to the 002 reflection from the parallel stacking of graphenes and with d_{002} values lying between 3.65 and 3.75 (Figure 8a−c). The broad 002 peaks can be ascribed to stacking of graphenes of small dimensions in a parallel fashion. In addition, broad peaks and d_{002} values greater than 3.34 Å of ideal graphite are characteristic of disordered and active carbons[45,46] with the higher the disorder the higher the d_{002} values. The width of the parallel stacking of graphenes can be estimated from the Scherrer formula.[18,47]

$$L_c = K\lambda/B\cdot\cos\theta$$

in which $\lambda = 1.54$ Å, K is the apparatus constant (≈1), and B is the half-width of the peak in radians. The L_c values of the present carbons do not present any significant differences and correspond to a maximum of two graphenes in parallel orientation. Nevertheless, a progressive decrease is observed from carbon (7.1 Å) >w-carbon (6.7 Å) > uw-carbon (5.5 Å). Since these samples differ only in the H_2SO_4 treatment, the change in the L_c values may be attributed to the role of H_2SO_4. As mentioned previously, the H_2SO_4 treatment promotes cross-linking and polymerization of sugar, leading to a carbon precursor that is difficult to graphitize with a single graphene fraction very high in the final product. This trend is demonstrated by the smaller L_c value for the uw-carbon product.

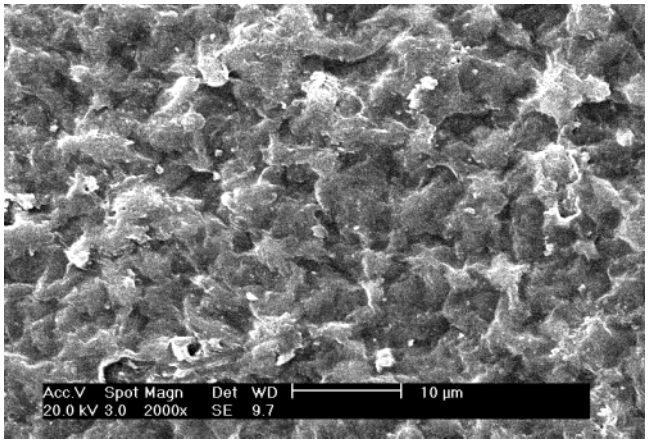

Figure 9. SEM image of the Z-H^+(w)/C composite, showing the characteristic "cornflakes" of the surfaces of the mineral.

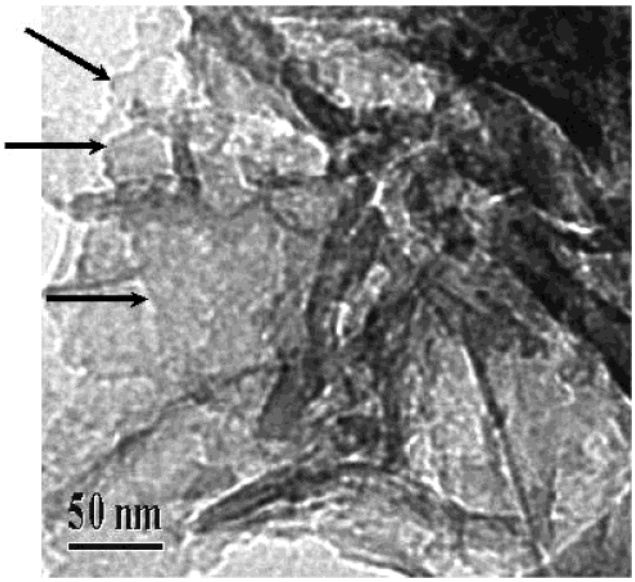

Figure 10. TEM micrograph of the uw-carbon; the arrows point to the edges of graphene layers.

Electron Microscopy. Figure 9 shows the texture of Z-H^+(w)/C composite deposited on graphite by scanning electron microscopy. The SEM image unveils the characteristic flexible sheet "cornflake" morphology of the surfaces formed by interconnected ridges and valleys. This pattern is very similar to that of montmorillonite.[48,49]

A TEM micrograph of the carbons derived after dissolution of mineral is shown in Figure 10. It is observed that graphenes adopt in some regions flat orientations forming discernible planar sheets with lateral extent ranging from about 30 to 80 nm. The black arrows in Figure 10 point out the edges of such sheets. These flat orientations can be described like a "mosaic" built up of tiny graphenes, measuring up to 10−30 Å, as evidenced by Figure 11. The flat orientation can be explained by accepting the template role of the clay layers during carbonization of sucrose inside the mineral. However, this template effect does not lead to long-range scale ordering of graphenes, and this is evident

(45) Dahn, J. R.; Xing, W.; Gao, Y. *Carbon* **1996**, *35*(6), 825.
(46) Yoshizawa, N.; Maruyama, K.; Yamada, Y.; Zielinska-Blajet, M. *Fuel* **2000**, *79*, 1461.
(47) Klug, H. P.; Alexander, L. E. *X-ray Diffraction Procedures for Polycrystaline and Amorphous Materials*, 2nd ed.; Wiley: New York, 1974; pp 687−690.
(48) King, R. D.; Nocera, D. G.; Pinnavaia, T. J. *Electranal. Chem.* **1987**, *236*, 43.
(49) Sondi, I.; Pravdić, V. *J. Colloid Interface Sci.* **1996**, *181*, 463.

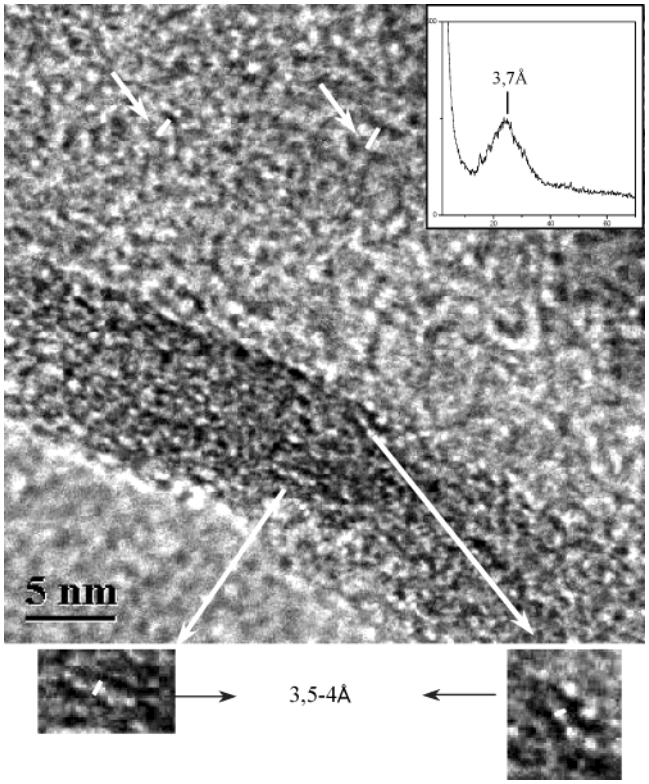

Figure 11. High-resolution TEM micrograph of the derived uw-carbon in the 002 lattice fringe mode; arrows show the distance between graphene sheets with a face to face orientation and the inset depicts the 002 diffraction peak in the XRD pattern.

from the lack of XRD reflections other than that of the (002) planes of graphenes, as was shown previously in Figure 8. Furthermore, the formation of these planar sheets of graphenes is another evidence of preservation of the layered aluminosilicate lattice in the clay/carbon composites after pyrolysis.

High-resolution TEM micrographs of the derived carbons provide further information about the structure of these products (Figure 11). The picture shows 002 graphene lattice fringes, which help to visualize the profile of the carbon layers. The lateral extent of graphenes from the carbonization of sucrose inside the inorganic substrate is estimated between 10 and 30 Å. This value is similar to that obtained from carbonization of pure sucrose.[50] Furthermore, two different regions of carbonaceous material are observed: One with spare packing of graphene sheets and the other with denser packing, the latter indicated by the darker stripe in Figure 11. The distance between graphene sheets in parallel orientation, indicated by arrows in the upper part of the micrograph, is estimated to be between 9 and 10 Å. This distance, which is close to the thickness of the montmorillonite layer (9.5 Å), confirms the template effect of the clay structure. On the other hand, the distance of graphene sheets in the region of dense packing lies between 3.5 and 4 Å, very similar to the distance estimated from the XRD measurements, and indicates disordered carbons. The above results suggest that carbonization takes place either inside the lamellar space of montmorillonite, producing graphenes separated by a distance dictated by the clay matrix, or outside the clay platelets, e.g. between two bundles of clay sheets, producing d_{002} values expected for disordered carbons. Finally, we note that the TEM results for the parallel stacking of graphenes are in agreement with those from XRD (L_c values), as no more than two graphenes can be observed in the HRTEM micrographs in parallel orientation.

Table 3. Specific Surface Areas of Composites and Derived Carbons

sample	S_{BET} (m^2/g)	S_{DRK} (m^2/g)	n_{DR}	E_{DR} (kJ/mol)	V_{mic} (cm^3/g)	V_{tot} (cm^3/g)
Z-Na^+	36	41	2.4	4.2	0.015	0.11
Z-Na^+/C	59	61	2.05	6.1	0.022	0.13
Z-H^+(w)/C	57	62	1.98	6.2	0.022	0.13
Z-H^+(uw)/C	521	574	2.00	7.5	0.204	0.41
carbon	680	676	2.01	6.2	0.241	0.95
w-carbon	659	681	2.00	6.1	0.242	0.97
uw-carbon	1290	1315	2.00	6.2	0.468	1.48
sug-H^+/600[a]	67−494					
CTC[b]	446	623			0.296	0.54

[a] From ref 54. [b] From ref 55

Nitrogen Adsorption Isotherms. Nitrogen adsorption isotherms carried out at 77 K, from the parent clay (Z-Na^+), clay/carbon composites, as well as the carbons derived, are shown in Figure 12. Additionally, the calculated (BET and DRK) specific surface areas, total pore volumes, and DR micropore volumes are cited in Table 3. Table 3 also contains the characteristic exponents (n_{DA}) and energy (E_{DA}), as calculated by fitting the initial part ($p/p_o < 0.1$) of the isotherms via the DA approach.[51]

The general shape of all isotherms suggests the existence of different pore sizes spanning from micro- to macropores. Specifically, the steep increase in the adsorbed volume sorbed at low relative pressures reveals the presence of microporosity in the solids, which is dramatically increased in the order clay < composite < carbon (see also data in Table 3). This immediately suggests that after the intercalation and pyrolysis of sucrose, new micropores are created, while the subsequent dissolution of the dense aluminosilicate clay sheets has a 2-fold effect, as it renders extra pore space accessible to N_2 molecules while it simultaneously reduces the apparent density of the solid. The following small slope observed at medium relative pressures as well as the desorption hysteresis denotes the presence of mesoporosity, while the final rising tail at relative pressures near 1 points to the possible presence of macropores.[51,52]

It is also noteworthy that the general shape of the isotherm pertaining to the parent clay is retained for all samples studied. Specifically, the H3 (according to IUPAC classification) type hysteresis loop, which is characteristic for the majority of smectite clay minerals and clay-based porous solids (e.g. pillared clays) and thus considered typical for layered materials with slit-shaped pores, is preserved in its original form. This suggests a "short-range scale" but strong templating effect of the parent clay, as both composites and carbons can be characterized as "high surface area clones" of the

(50) Buiel, E. R.; George, A. E.; Dahn, J. R. *Carbon* **1999**, *37*, 1339.

(51) Gregg, S. J.; Sing, K. S. W. *Adsorption, Surface Area and Porosity*; Academic Press: London, 1991.

(52) Lowell, S.; Shields, J. E. *Powder Surface Area and Porosity*, 3d ed.; Chapman & Hall, New York, 1991.

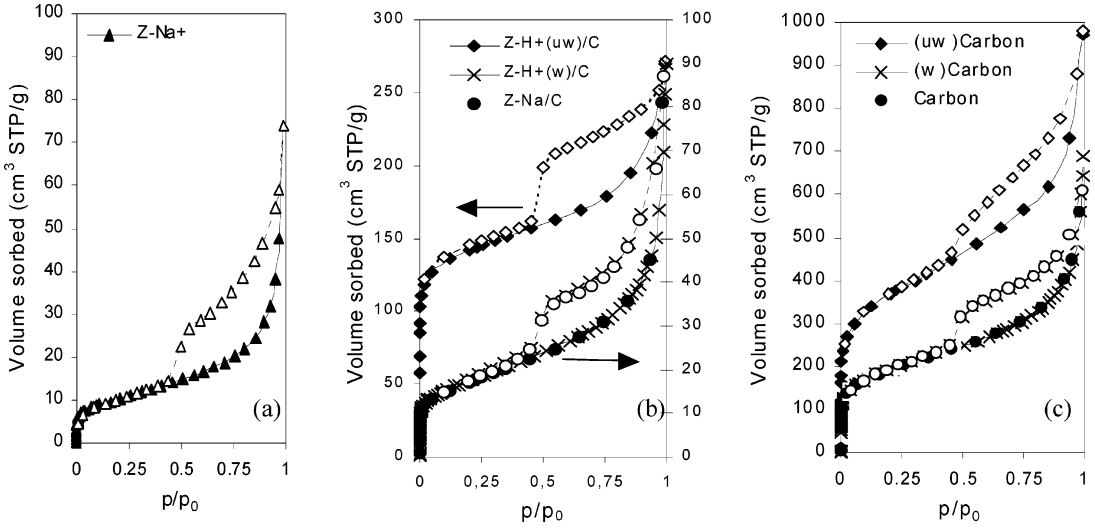

Figure 12. N_2 adsorption isotherms at 77 K, of (a) Z-Na^+ montmorillonite (parent clay), (b) clay/carbon composites, with arrows indicating the different scale axis, and (c) derived carbons. Solid symbols and lines, adsorption; open symbols and dashed lines, desorption.

clay. We use the term "short-range scale" because the X-ray diffractograms of produced carbons do not show any ordering that could be connected to a long-range scale resemblance to the phyllomorphic pattern of the clays. It must be noted that uw-carbon differs slightly from this general picture as the hysteresis loop develops gradually, suggesting the development of a wider mesopore size distribution including larger pores. Similar nitrogen isotherms have been reported for mesoporous clays and pillared clays based on Laponite, a synthetic montmorillonite with very small platelets (<0.1 mm) that favor the house of cards structure and thus mesoporosity.[53]

It is also clear, after comparison of the washed [Z-H^+-(w)/C and w-carbon] with the unwashed [Z-H^+(uw)/C and uw-carbon] samples (Figure 12), that the treatment with H_2SO_4 increases the N_2 adsorption capacity and surface areas of both the composite and the derived carbon. The total pore volume is also greatly increased by the use of H_2SO_4 from approximately 0.140 cm^3/g for composites Z-H^+(w)/C and Z-Na^+/C to 0.420 cm^3/g for Z-H^+(uw)/C and from 0.872 and 1.06 for carbon and w-carbon to 1.503 for uw-carbon. It is interesting to note that the BET surface area of the uw-carbon (1290 m^2/g) is almost 2 times higher than those reported from carbonization of pure sugar with or without H_2SO_4 activation[54] and bentonite-templated furfuryl alcohol based activated carbon (CTC).[55]

The reliable assessment of pore size distributions, especially for micropores, is yet to be resolved, as the mechanisms of molecular adsorption are still under active debate. The complete and comprehensive analysis of the pore network of the derived materials as well as comparative studies on different approaches for the pore size distributions are beyond the scope of this work. For the sake of comparison, we have chosen to present two common approaches, namely the Dubinin−Astakhov[56] (DA) and the Barett−Joyner−Halenda[51] (BJH) methods, concerning the micropore and mesopore ranges, respectively. The above approaches were used in their "slit-pore" variants; for the DA approach, only the low-pressure part of the isotherm ($p/p_0 < 0.01$) was fitted, while the mid- and high-pressure parts ($0.3 < p/p_o < 1$) of the desorption branches were used for BJH analysis; the Halsey standard isotherm[52] was used as reference for the calculation of adsorbed film thickness. Knowing the limitations of these methods, it should be explicitly mentioned that the results are to be used for comparison only and not to represent actual pore sizes.

Based on BJH analysis, the mean mesopore width for all the materials under consideration (i.e. parent clay, composite materials and carbons) is approximately 26 Å, as shown by the distributions of Figure 13 (right). This size is actually an artifact related to the hysteresis loop closing point, which in turn relates to the tensile strength of liquid N_2. It is evident that large mesopores (up to 100 Å) and finer pores (w < 26 Å) are created after the removal of the clay. The pore size distribution of uw-carbon is much broader, as expected from the smoother desorption curves. A very interesting point is the "unique" small structure observed at around 32 Å (Figure 13, arrow), which can be attributed to pore widening from the cooperative action of the H_2SO_4 and the etching of the inorganic substrate. In the micropore region, the DA method (Figure 13, left) gave almost identical pore size distributions centered at around 7.5 Å for all the samples. In general, the DA approach is not very sensitive to small differences in pore sizes; however, the noticeable difference in the distribution shape between the washed and unwashed composites and the derived carbons implies smaller micropores in the unwashed products, supported also by the slightly higher characteristic energy (see Table 3), which are broadened upon removal of the clay.

(53) Butruille, J.-R.; Pinnavaia, T. J. *Multifunctional Mesoporous Inorganic Solids*; Sequeira, C. A. C., Hudson, M. J., Eds.; NATO ASI Series C, 1993; Vol. 400, pp 359−372.

(54) Xing, W.; Xue, J. S.; Dahn, J. R. *J. Electrochem. Soc.* **1996**, *143*, 3046.

(55) Barata-Rodrigues, P. M.; Mays, T. J.; Moggridge, G. D. *Carbon* **2003**, *41*, 2231

(56) Dubinin, M. M. In *Characterization of porous solids*; Gregg S. J., Sing K. S., Stoeckli, F., Eds.; Soc. Chem. Ind.: London, 1979; pp 1−11.

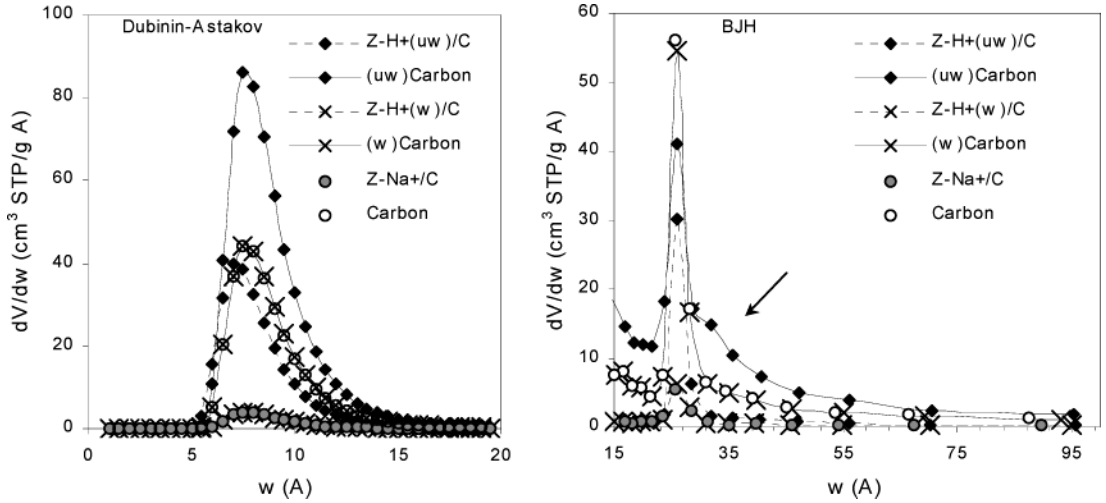

Figure 13. Pore width distributions of the products: (left) DA method (w < 20 Å) and (right) BJH method (w > 15 Å).

Conclusions and Perspectives

The present results demonstrate that the clay−carbon composites synthesized in this work are stable hybrid materials, with graphenes occupying the interlayer space and coating the clay platelets. The composites exhibit increased thermal stability, which is attributed to the shielding effect of graphenes. Results also show that H_2SO_4 activation during pyrolysis, in conjunction with a short-range scale templating effect of the clay substrate, is essential for improving the N_2 adsorption properties of the products. The HRTEM micrographs from the derived carbons unveil the role of the inorganic substrate and indicate loose packing ordering of graphenes, leading to improved surface areas. Finally, the use of clays with an in situ treatment with H_2SO_4 offers the advantage to produce clay−carbon activated composite in bulk, in contrast to activation by steam or other gas that often leave the core of the solid granules unaffected.[40] The present composite materials possess mesoporosity and possibly macroporosity, properties desirable for catalytic, environmental, and other applications.

Acknowledgment. We gratefully acknowledge the assistance of Mr. T. Szabo, Department of Colloid Chemistry, University of Szeged, Hungary, for the thermogravimetric measurements.

Supporting Information Available: TG diagrams of the three final composites in oxygen atmosphere are available in PDF format free of charge via the Internet at http://pubs.acs.org.

CM0350030